ELSEVIER

International Journal of Solids and Structures 41 (2004) 5631–5645

INTERNATIONAL JOURNAL OF SOLIDS and STRUCTURES

www.elsevier.com/locate/ijsolstr

Impact response of a surface crack in a coating/substrate system with a functionally graded interlayer: antiplane deformation

Hyung Jip Choi *

School of Mechanical and Automotive Engineering, Kookmin University, 861-1 Chongnung-dong, Songbuk-gu, Seoul 136-702, Republic of Korea

Received 13 November 2003; received in revised form 19 February 2004
Available online 1 June 2004

Abstract

In this paper, the elastodynamic crack problem for a coating/substrate system with a functionally graded interfacial zone is investigated under the condition of antiplane shear impact. With the interfacial zone being modeled by a nonhomogeneous interlayer having the power-law variations of shear modulus and mass density, the coating is assumed to contain an embedded or an edge crack perpendicular to the boundaries. Laplace and Fourier integral transforms are used to reduce the transient problem to solving a singular integral equation with a generalized Cauchy kernel in the Laplace transform domain. The time dependence of the crack-tip response in the physical domain is recovered via the numerical inversion of the Laplace transforms and the values of dynamic mode III stress intensity factors are provided as a function of time. As a result, the effects of material and geometric parameters of the current coating/substrate system on the dynamic load transfer and overshoot characteristics over the corresponding elastostatic solutions are addressed.

Keywords: Coating/substrate system; Surface crack; Functionally graded materials; Interfacial zone; Dynamic stress intensity factors

1. Introduction

The use of functionally graded materials in a wide range of modern engineering practice has been rapidly increasing over the past decade, taking advantage of their attractive traits of relatively smooth spatial variations of physical properties (Suresh and Mortensen, 1998). The deliberate use of graded media, among other applications, in the form of an interlayer as a distinctive transition phase between the incompatible dissimilar constituents can aid in soothing out the property mismatch that is apparent across the materials juncture. It is thus feasible to achieve the enhanced reliability and durability over the conventional,

* Tel.: +82-2-910-4682; fax: +82-2-910-4839.
E-mail address: hjchoi@kookmin.ac.kr (H.J. Choi).

0020-7683/$ - see front matter © 2004 Elsevier Ltd. All rights reserved.
doi:10.1016/j.ijsolstr.2004.04.020

discretely layered or coated system (Miyamoto et al., 1999). At the same time, many challenging issues have arisen in connection with the fatigue and fracture behavior of functionally graded materials, which have prompted extensive research demands for finding the solutions to some related crack problems under various loading conditions. A review of previous investigations, along with a number of salient features encountered in the analysis of such crack problems entailing the graded, nonhomogeneous properties, can be found in the article by Erdogan (1998).

When it comes to the situations where the external loading is dynamic in nature, a subject area of substantial importance would be to study the impact response of the graded media containing crack-like flaws. In this regard, Babaei and Lukasiewicz (1998) evaluated the dynamic stress intensity factors for an antiplane shear crack in a graded material between the dissimilar half-planes, and Li et al. (2001) and Li and Weng (2002) examined the torsional impact behavior of a cylindrical crack and a penny-shaped crack, respectively, in the graded interlayer. More recently, the impact failure of a mode III crack located parallel to the boundaries of a graded orthotropic strip was predicted by Feng et al. (2003) based on the energy density criterion, whereas the dynamic response of a mode I crack perpendicular to the free surfaces of a nonhomogeneous orthotropic strip was considered by Chen et al. (2002). Another example of transient fracture analysis is that of a mode III crack in an unbounded functionally graded material using the boundary integral equation method performed by Zhang et al. (2003), where the variations of elastic properties were described by both the unidirectional and bidirectional exponential laws. Instead of taking the material parameters of the graded constituents to be certain continuous functions, i.e., exponential or power functions of space as in the aforementioned, Wang et al. (2000) proposed a multilayered composite model to provide the elastodynamic solutions for some cracked specimens possessing the graded, nonhomogeneous properties. To be specific, the graded region was simulated as the sum of several sublayers with slightly different homogeneous properties in each sublayer. This approach was employed independently by Itou (2001) for the dynamic analysis of a mixed mode crack in a nonhomogeneous interfacial layer between two dissimilar half-planes. Similarly, but in contrast to having piecewise constant elastic properties, Wang and Gross (2000) assigned the shear modulus that varies linearly in each sublayer and is continuous on the subinterfaces, with application to a dynamic mode III crack in a graded interfacial layer of bonded materials.

The objective of this paper is to investigate the impact response of an embedded or an edge crack in a coating/substrate system with a graded interfacial zone subjected to the antiplane shear loading condition. The interfacial zone in-between is modeled by a nonhomogeneous interlayer with the spatially varying shear modulus and mass density in terms of power functions. The method of analysis is based on the use of Laplace and Fourier integral transforms, coupled with the solution of a resulting singular integral equation with a generalized Cauchy kernel in the Laplace transform domain. The particular emphasis is placed on determining the mode III stress intensity factors, which are first defined and estimated in the Laplace transform domain. Subsequently, the crack-tip response in the physical domain is recovered by the numerical Laplace inversion, leading to the evaluation of dynamic mode III stress intensity factors as a function of time for various combinations of material and geometric parameters of the problem under consideration. Further attention is also paid to the dynamic overshoot characteristics over the corresponding elastostatic solutions.

2. Problem description and basic equations

Consider a coating/substrate system with a graded interfacial zone as shown in Fig. 1, where the coating on the left-hand side contains a crack of length $2c = b - a$ perpendicular to the boundaries. By modeling the interfacial zone in-between as a nonhomogeneous interlayer, the quantities associated with the cracked coating, the interlayer, and the substrate are defined in the local coordinates $(x, y) = (x_j, y)$, $j = 1, 2, 3$, with

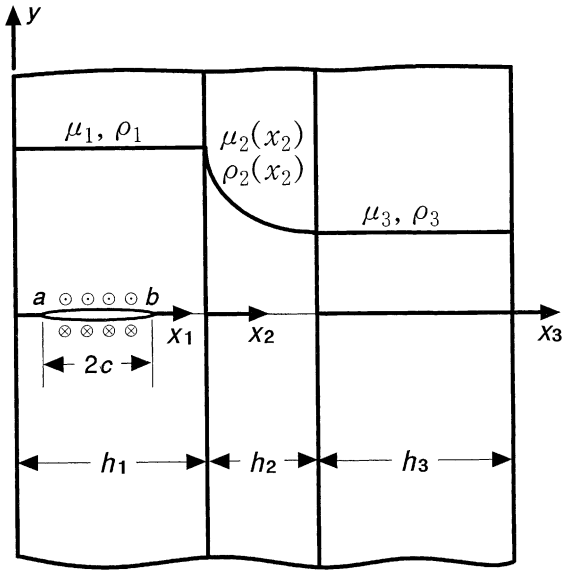

Fig. 1. Configuration of a cracked coating/substrate system with a functionally graded interfacial zone.

the thicknesses being h_j, $j = 1, 2, 3$, respectively. It is assumed that the coated system, which is initially at rest and stress-free, is suddenly exposed to an antiplane shear traction applied on the crack surface. With shear moduli and mass densities of the homogeneous constituents given by μ_j and ρ_j, $j = 1, 3$, respectively, those of the nonhomogeneous interlayer are expressed as (Chiu and Erdogan, 1999)

$$\mu_2(x) = \mu_1(1 + \alpha x)^{\beta}, \quad \rho_2(x) = \rho_1(1 + \alpha x)^{\beta-2}, \tag{1}$$

where the constant α and the exponent β are determined in the local coordinates $(x, y) = (x_2, y)$ so as to render the continuous transition of such properties at the locations of nominal interfaces such that

$$\alpha = \frac{\sqrt{\mu_3/\mu_1} - \sqrt{\rho_3/\rho_1}}{h_2\sqrt{\rho_3/\rho_1}}, \quad \beta = \frac{2\ln(\mu_3/\mu_1)}{\ln(\mu_3/\mu_1) - \ln(\rho_3/\rho_1)}. \tag{2}$$

With $w_j(x, y, t)$, $j = 1, 2, 3$, denoting the z-component of the displacement vector under antiplane shear deformation, the corresponding stress components are given by

$$\tau_{jxz} = \mu_j \frac{\partial w_j}{\partial x}, \quad \tau_{jyz} = \mu_j \frac{\partial w_j}{\partial y}, \qquad j = 1, 2, 3 \tag{3}$$

and the equations of motion for the constituents of the 3-layer coating/substrate system are written as

$$\nabla^2 w_j = \frac{\rho_j}{\mu_j} \frac{\partial^2 w_j}{\partial t^2}, \quad j = 1, 3, \tag{4}$$

$$\nabla^2 w_2 + \frac{\alpha\beta}{1 + \alpha x} \frac{\partial w_2}{\partial x} = \frac{\rho_1}{\mu_1(1 + \alpha x)^2} \frac{\partial^2 w_2}{\partial t^2}, \tag{5}$$

where t is the time and ∇^2 is the two-dimensional Laplacian operator in the variables x and y.

Because the geometric and material symmetry prevails with respect to x-axis, only the upper half of the region, $y > 0$, is considered. Together with the initial conditions as follows:

$$w_j(x_j,y,0)=0,\quad \frac{\partial w_j}{\partial t}(x_j,y,0)=0,\qquad 0<x_j<h_j,\quad j=1,2,3. \tag{6}$$

the conditions of traction-free boundaries and perfect bonding along the nominal interfaces in the coated system are imposed in the local coordinates as

$$\tau_{1xz}(0,y,t)=0,\quad \tau_{3xz}(h_3,y,t)=0, \tag{7}$$

$$w_1(h_1,y,t)=w_2(0,y,t),\quad w_2(h_2,y,t)=w_3(0,y,t), \tag{8}$$

$$\tau_{1xz}(h_1,y,t)=\tau_{2xz}(0,y,t),\quad \tau_{2xz}(h_2,y,t)=\tau_{3xz}(0,y,t) \tag{9}$$

and the mixed conditions on the plane of the crack, $y=0$, are prescribed as

$$w_j(x_j,0,t)=0,\quad 0<x_j<h_j,\ \ j=2,3, \tag{10}$$

$$w_1(x_1,0,t)=0,\quad 0<x_1<a,\ \ b<x_1<h_1, \tag{11}$$

$$\tau_{1yz}(x_1,0,t)=f(x_1)H(t),\quad a<x_1<b, \tag{12}$$

where $f(x_1)$ is the arbitrary crack surface traction and $H(t)$ refers to the Heaviside unit step function.

A pair of Laplace transform and its inverse over the time variable t is defined as (Churchill, 1981)

$$w_j^*(x_j,y,p)=\int_0^\infty w_j(x_j,y,t)\mathrm{e}^{-pt}\,\mathrm{d}t,\quad w_j(x_j,y,t)=\frac{1}{2\pi\mathrm{i}}\int_{Br} w_j^*(x_j,y,p)\mathrm{e}^{pt}\,\mathrm{d}p, \tag{13}$$

where p is the Laplace transform variable, Br stands for the Bromwich path of integration, and $\mathrm{i}=(-1)^{1/2}$.

Upon applying the Laplace transform, the time dependence is eliminated from the equations of motion so that the general solutions for the displacement components, $w_j^*(x,y,p)$, $j=1,2,3$, can be obtained in terms of the Fourier integrals in the local coordinates $(x,y)=(x_j,y)$, $j=1,2,3$, as

$$w_1^*(x,y,p)=\frac{2}{\pi}\int_0^\infty (A_1\mathrm{e}^{\lambda_1 x}+A_2\mathrm{e}^{-\lambda_1 x})\sin sy\,\mathrm{d}s+\frac{1}{2\pi}\int_{-\infty}^\infty \mathrm{e}^{-\lambda_1 y-\mathrm{i}sx}\,\mathrm{d}s,\quad 0<x<h_1, \tag{14}$$

$$w_2^*(x,y,p)=\frac{2}{\pi}(1+\alpha x)^{(1-\beta)/2}\int_0^\infty\left[B_1 I_v\left[\frac{s}{|\alpha|}(1+\alpha x)\right]+B_2K_v\left[\frac{s}{|\alpha|}(1+\alpha x)\right]\right]\sin sy\,\mathrm{d}s,\quad 0<x<h_2, \tag{15}$$

$$w_3^*(x,y,p)=\frac{2}{\pi}\int_0^\infty (C_1\mathrm{e}^{\lambda_3 x}+C_2\mathrm{e}^{-\lambda_3 x})\sin sy\,\mathrm{d}s,\quad 0<x<h_3, \tag{16}$$

where s is the Fourier transform variable, $A_j(s,p)$, $j=1,2,3$, $B_j(s,p)$, $C_j(s,p)$, $j=1,2$, are arbitrary unknown functions to be determined, and $I_v(\ )$ and $K_v(\ )$ are the modified Bessel functions of the first and second kind, respectively, with $\lambda_j(s,p)$, $j=1,3$, and $v(p)$ written as

$$\lambda_j=\sqrt{s^2+\frac{\rho_j}{\mu_j}p^2},\quad j=1,3;\qquad v=\sqrt{\left(\frac{1-\beta}{2}\right)^2+\frac{\rho_1}{\mu_1}\left(\frac{p}{\alpha}\right)^2} \tag{17}$$

and the expressions for the corresponding stress components are obtainable in the Laplace transform domain from the constitutive relations in Eq. (3).

3. Derivation of the integral equation

In order to derive the integral equation for the crack problem, a new unknown function is introduced in the Laplace transform domain to replace the mixed conditions in Eqs. (11) and (12), i.e.,

$$\phi^*(x_1,p)=\begin{cases}\dfrac{\partial}{\partial x_1}w_1^*(x_1,0,p), & a<x_1<b,\\ 0, & 0<x_1<a,\ \ b<x_1<h_1\end{cases} \tag{18}$$

and the boundary and interface conditions in Eqs. (7)–(9) and (12) to be met in the Laplace transform domain are rewritten as

$$\tau_{1xz}^*(0,y,p)=0,\quad \tau_{3xz}^*(h_3,y,p)=0, \tag{19}$$

$$w_1^*(h_1,y,p)=w_2^*(0,y,p),\quad w_2^*(h_2,y,p)=w_3^*(0,y,p), \tag{20}$$

$$\tau_{1xz}^*(h_1,y,p)=\tau_{2xz}^*(0,y,p),\quad \tau_{2xz}^*(h_2,y,p)=\tau_{3xz}^*(0,y,p), \tag{21}$$

$$\tau_{1yz}^*(x_1,0,p)=\frac{f(x_1)}{p},\quad a<x_1<b. \tag{22}$$

It is then observed from Eqs. (14) and (18) that the expression for the unknown $A_3(s,p)$ is obtained as

$$A_3(s,p)=\frac{\mathrm{i}}{s}\int_a^b \phi^*(r,p)\mathrm{e}^{\mathrm{i}sr}\,\mathrm{d}r \tag{23}$$

and those for the six other unknowns, $A_j(s,p)$, $B_j(s,p)$, and $C_j(s,p)$, $j=1,2$, can be also determined in terms of ϕ^* by the applications of Eqs. (19)–(21). Hence, the auxiliary function ϕ^* becomes the only unknown to be evaluated in such a way that the crack surface condition in Eq. (22) is satisfied.

Subsequently, from Eqs. (3) and (14) and using the required expressions for $A_j(s,p)$, $j=1,2,3$, followed by some algebraic manipulations, the traction component, τ_{1yz}^*, along the crack plane can be written in the form as

$$\frac{\pi}{\mu_1}\lim_{y\to+0}\tau_{1yz}^*(x,y,p)=\int_a^b [K_1(x,r,p)+K_2(x,r,p)]\phi^*(r,p)\,\mathrm{d}r,\quad x>0, \tag{24}$$

where $K_j(x,r,p)$, $j=1,2$, are the kernels such that

$$K_1(x,r,p)=-\frac{\mathrm{i}}{2}\int_{-\infty}^{\infty} R(s,p)\mathrm{e}^{\mathrm{i}s(r-x)}\,\mathrm{d}s, \tag{25}$$

$$K_2(x,r,p)=\int_0^{\infty} Q(x,r,s,p)\,\mathrm{d}s, \tag{26}$$

with the integrands $R(s,p)$ and $Q(x,r,s,p)$ being given by

$$R(s,p)=\frac{1}{s}\sqrt{s^2+\frac{\rho_1}{\mu_1}p^2}, \tag{27}$$

$$Q(x,r,s,p)=\frac{s^2}{\lambda_1^2}[\mathrm{e}^{-\lambda_1(x+r)}+4\mathrm{e}^{-\lambda_1 h_1}\Delta_0(s,p)\cosh\lambda_1 x\sinh\lambda_1 r] \tag{28}$$

in which the expression for the function $\Delta_0(s,p)$ can be found in Appendix A.

Upon identifying the asymptotic properties of the integrands for large values of the variable s

$$\lim_{|s|\to\infty} R(s,p) = R_\infty(s) = \frac{|s|}{s}, \tag{29}$$

$$\lim_{s\to\infty} Q(x,r,s,p) = Q_\infty(x,r,s) = \mathrm{e}^{-s(x+r)}. \tag{30}$$

It is therefrom obvious that the singularities the kernels may have must be the consequence of the foregoing limiting behavior as s tends to infinity.

As a result, after separating the singular parts from the kernels and applying the crack surface condition in Eq. (22), an integral equation is derived that is valid for both the embedded ($a > 0$) and the edge crack ($a = 0$) such that

$$\int_a^b \left[\frac{1}{r-x} + \frac{1}{r+x} + G(x,r,p)\right]\phi^*(r,p)\,\mathrm{d}r = \frac{\pi}{\mu_1}\frac{f(x)}{p}, \quad a < x < b, \tag{31}$$

where the kernel $G(x,r,p)$ is written as

$$G(x,r,p) = \int_0^\infty [R(s,p) - R_\infty(s)]\sin s(r-x)\,\mathrm{d}s + \int_0^\infty [Q(x,r,s,p) - Q_\infty(x,r,s)]\,\mathrm{d}s. \tag{32}$$

It should be mentioned that when the crack is embedded as $a > 0$, the term $1/(r-x)$ in Eq. (31) is known as a Cauchy singular kernel that leads to the standard square-root singularity for the unknown function ϕ^* and the other two terms inside the bracket of Eq. (31) remain bounded in the closed interval $[a,b]$, without affecting the singular behavior of crack-tip stresses. For the case of an edge crack problem as $a = 0$, besides the Cauchy kernel that is singular at $x = r$, the term $1/(r+x)$ becomes also unbounded when x and r approach the zero end point simultaneously, while the function $G(x,r,p)$ is a regular kernel. In this case, the first two terms in the kernels of the integral equation constitute a generalized Cauchy singular kernel.

4. Solution of the integral equation

The dominant singular kernel in the integral equation is the Cauchy-type for both cases of the embedded and the edge crack. This also holds true even for the crack that terminates at the nominal interface with the graded interlayer, i.e., $b = h_1$, where the continuity of shear moduli exists (Erdogan, 1998). The auxiliary function ϕ^* for these two crack configurations can therefore be expressed as (Muskhelishvili, 1953)

$$\phi^*(r,p) = \begin{cases} \dfrac{g(r,p)}{\sqrt{(r-a)(b-r)}}, & a < r < b, \\ \dfrac{g(r,p)}{\sqrt{b-r}}, & 0 < r < b, \end{cases} \tag{33}$$

where $g(r,p)$ is an unknown function bounded and nonzero at the end points.

After normalizing the interval from (a,b) to $(-1,1)$ such that

$$\begin{Bmatrix} r \\ x \end{Bmatrix} = \frac{b-a}{2}\begin{Bmatrix} \eta \\ \xi \end{Bmatrix} + \frac{b+a}{2}, \quad -1 < (\xi,\eta) < 1, \tag{34}$$

the solution to the integral equation can be expanded into the following series:

$$\phi^*(\eta,p)=\begin{cases}\dfrac{1}{p\sqrt{1-\eta^2}}\displaystyle\sum_{n=0}^{\infty}c_nT_n(\eta); & |\eta|<1,\ \ a>0\\ \dfrac{1}{p\sqrt{1-\eta}}\displaystyle\sum_{n=0}^{\infty}c_nT_n(\eta); & |\eta|<1,\ \ a=0\end{cases} \tag{35}$$

where T_n is the Chebyshev polynomial of the first kind and c_n, $n\geqslant 0$, are coefficients to be determined. It is to be pointed out that for the embedded crack, the function ϕ^* must fulfill the single-valuedness as

$$\int_{-1}^{1}\phi^*(\eta,p)\,\mathrm{d}\eta=0 \tag{36}$$

and from the first of Eq. (35) and Eq. (36) and the orthogonality of T_n, it can be seen that $c_0=0$. In the edge crack problem, however, the solution to the integral equation no longer contains an arbitrary constant so that the compatibility condition as above is not needed in ensuring a unique solution.

Upon substituting Eqs. (34) and (35) into Eq. (31), truncating the series with a finite number of terms, and using the properties of the Chebyshev polynomials (Gradshteyn and Ryzhik, 1980)

$$\int_{-1}^{1}\frac{T_n(\eta)}{\sqrt{1-\eta^2}(\eta-\xi)}\,\mathrm{d}\eta=\pi U_{n-1}(\xi),\quad |\xi|<1,\ \ n\geqslant 1, \tag{37}$$

$$\int_{-1}^{1}\frac{T_n(\eta)}{\sqrt{1-\eta}(\eta-\xi)}\,\mathrm{d}\eta=\int_{-1}^{1}\frac{T_n(\eta)-T_n(\xi)}{\sqrt{1-\eta}(\eta-\xi)}\,\mathrm{d}\eta+\frac{T_n(\xi)}{\sqrt{1-\xi}}\ln\left|\frac{1+\sqrt{(1-\xi)/2}}{1-\sqrt{1-\xi/2}}\right|,\quad |\xi|<1,\ \ n\geqslant 0, \tag{38}$$

where U_n is the Chebyshev polynomial of the second kind, the integral equation can be regularized. The ensuing functional equation can be recast into a system of linear algebraic equations for the unknown coefficients c_n. To this end, the roots of the Chebyshev polynomial of the first kind are employed as a set of collocation points (Erdogan, 1998), together with the involved bounded integrals evaluated by using the appropriate Gaussian quadrature rules (Davis and Rabinowitz, 1984).

Once the coefficients c_n are determined, the integral equation in Eq. (31) provides the values of singular traction ahead of the crack tip. It may be worth reminding that when the elastic properties are continuous and piecewise differentiable near and at the crack tip, the corresponding stress field retains the square-root singularity and the structure which are the same as those in the homogeneous material (Eischen, 1987; Jin and Noda, 1994). As a result, the elevation of local crack-tip stresses can be extracted by first defining and evaluating the stress intensity factors in the Laplace transform domain as

$$K^*_{\mathrm{III}a}(p)=\lim_{x\to a^-}\sqrt{2(a-x)}\tau^*_{1yz}(x,0,p)=\begin{cases}\dfrac{\mu_1}{p}\sqrt{\dfrac{b-a}{2}}\displaystyle\sum_{n=1}^{N}(-1)^nc_n, & a>0,\\ 0, & a=0,\end{cases} \tag{39}$$

$$K^*_{\mathrm{III}b}(p)=\lim_{x\to b^+}\sqrt{2(x-b)}\tau^*_{1yz}(x,0,p)=\begin{cases}-\dfrac{\mu_1}{p}\sqrt{\dfrac{b-a}{2}}\displaystyle\sum_{n=1}^{N}c_n, & a>0,\\ -\dfrac{\mu_1}{p}\sqrt{b}\displaystyle\sum_{n=0}^{N}c_n, & a=0,\end{cases} \tag{40}$$

which is then followed by the numerical Laplace inversion to recover the time dependence of the stress intensifications, based on the algorithm developed by Stehfest (1970) such that

$$K_{\mathrm{III}a}(t)\cong\frac{\ln 2}{t}\sum_{m=1}^{M}V_mK^*_{\mathrm{III}a}\left(\frac{m}{t}\ln 2\right),\quad t>0, \tag{41}$$

$$K_{\mathrm{III}b}(t) \cong \frac{\ln 2}{t} \sum_{m=1}^{M} V_m K^*_{\mathrm{III}b}\left(\frac{m}{t} \ln 2\right), \quad t > 0, \tag{42}$$

where $K_{\mathrm{III}a}(t)$ and $K_{\mathrm{III}b}(t)$ are the dynamic mode III stress intensity factors at a specific time t for the crack tips a and b, respectively, M is a positive even number, and V_m is given by

$$V_m = (-1)^{m+M/2} \sum_{k=(1+m)/2}^{\min(m,M/2)} \frac{k^{M/2}(2k)!}{(M/2-k)!k!(k-1)!(m-k)!(2k-m)!}. \tag{43}$$

At large times, the values of such transient stress intensity factors would converge to those of the elastostatic solutions

$$\lim_{t\to\infty}[K_{\mathrm{III}a}(t), K_{\mathrm{III}b}(t)] \cong [(K_{\mathrm{III}a})_{\mathrm{static}}, (K_{\mathrm{III}b})_{\mathrm{static}}] \tag{44}$$

and these static limits can be obtained from the final-value theorem as (Churchill, 1981)

$$[(K_{\mathrm{III}a})_{\mathrm{static}}, (K_{\mathrm{III}b})_{\mathrm{static}}] = \lim_{p\to 0+} p[K^*_{\mathrm{III}a}(p), K^*_{\mathrm{III}b}(p)]. \tag{45}$$

To be mentioned is that due to the continuity of shear moduli and mass densities through the graded interlayer, the defined stress intensity factors are equally applicable even when the crack-tip intersects the nominal interface with the interlayer such that $b = h_1$.

5. Results and discussion

The integral equation in Eq. (31) is solved under the condition of uniform antiplane shear impact applied on the crack surface as $f(x_1) = -\tau_0$ in Eq. (12), with 30-term expansion of the auxiliary function in Eq. (35) and 10-term expansion for the inversion of the Laplace transforms in Eqs. (41) and (42). This numerical scheme leads to the solutions with a sufficient degree of accuracy for the material and geometric configurations considered in the present study. The resulting values of the normalized dynamic stress intensity factors, $K_{\mathrm{III}}(t)/\tau_0 l^{1/2}$, are plotted in Figs. 2–6 as a function of dimensionless time $t_* = c_s t/l$ for various

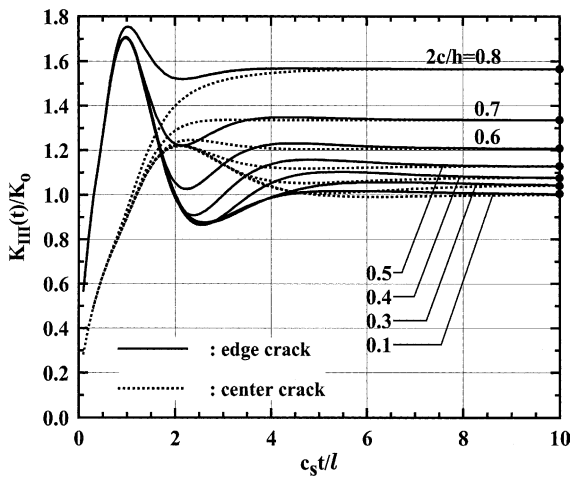

Fig. 2. Normalized dynamic stress intensity factors $K_{\mathrm{III}}(t)/K_0$ versus dimensionless time $c_s t/l$ for a homogeneous strip with a center or an edge crack ($K_0 = \tau_0 c^{1/2}$ and $l = c$ for the center crack; $K_0 = \tau_0 b^{1/2}$ and $l = 2c = b$ for the edge crack).

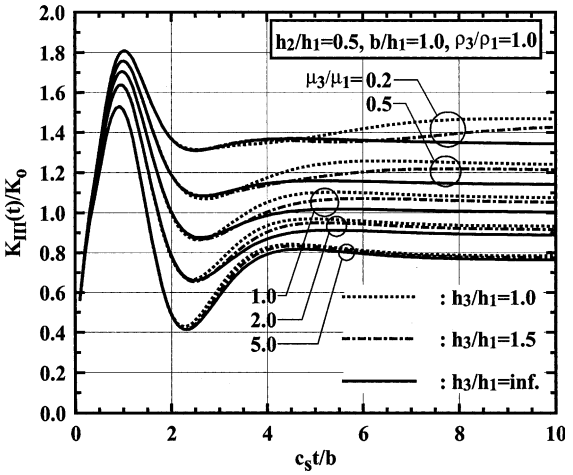

Fig. 3. Normalized dynamic stress intensity factors $K_{III}(t)/K_0$ of an edge crack as a function of dimensionless time $c_s t/b$ for different values of μ_3/μ_1 and h_3/h_1 ($K_0 = \tau_0 b^{1/2}$, $h_2/h_1 = 0.5$, $b/h_1 = 1.0$, $\rho_3/\rho_1 = 1.0$).

combinations of material $(\mu_3/\mu_1, \rho_3/\rho_1)$. and geometric parameters $(h_2/h_1, h_3/h_1, 2c/h_1)$ of the problem, where $l = c$ for the internal crack, $l = 2c = b$ for the edge crack, and $c_s = (\mu_1/\rho_1)^{1/2}$ is the shear wave velocity in the coating.

In order to discuss the results, it may be now appropriate to recall some general qualitative arguments from the elastodynamic crack problem. Namely, the impact-induced dynamic stress intensity factors rise rapidly with time, reach the peaks, and then decrease in magnitude, eventually settling down to the static limits for sufficiently large times. Such a generic feature can be attributed to the interactions between the waves scattered from the crack and those reflected from the boundaries and/or interfaces in the composite media (Sih and Chen, 1981). Further addressed in this section are the dynamic overshoot characteristics of the transient crack-tip behavior as quantified in Tables 1–5 by extracting the ratios between the peaks and the corresponding elastostatic solutions, $(K_{III})_{peak}/(K_{III})_{static}$.

The dynamic stress intensity factors for a homogeneous strip containing a center or an edge crack are first illustrated in Fig. 2 for different values of $2c/h$, where $h = h_1 + h_2 + h_3$ is the strip width, together with solid circles being added to represent the exact elastostatic solutions $K_{III}(\infty)/K_0 = [(h/\pi c)\tan(\pi c/h)]^{1/2}$ (Murakami, 1987). In this case, $\mu_3/\mu_1 = 1.0$ and $\rho_3/\rho_1 = 1.001$ are used to avoid the division by zero in Eq. (2) and it should be remarked that the current results for the center crack are in good agreement with those given by Chen (1977). It is apparent by comparison that the edge-cracked strip is subjected to the greater peaks of the normalized dynamic stress intensities than the center-cracked one. Of interest is that when $2c/h < 0.5$ for the embedded crack and $2c/h < 0.7$ for the edge crack, the peaks remain nearly the same for each crack problem. Table 1 provides the ratio of $(K_{III})_{peak}/(K_{III})_{static}$ that is seen to become enlarged when $2c/h$ decreases, implying the effect of inertia more dominant over the effect of finite geometry for the smaller crack size. When $2c/h$ is increased, however, the peak values approach the static limits. Also obvious from this table is the more pronounced dynamic overshoot for the edge crack. Based on the above and the general notion that the problem of edge cracking is of greater practical importance than that of the embedded crack, the results in the sequel are those for $a = 0$, i.e., $2c = b$.

The evolution of the dynamic stress intensity factors with time is given in Fig. 3 for several combinations of shear modulus ratio μ_3/μ_1 and relative substrate thickness h_3/h_1, with other properties being fixed as $h_2/h_1 = 0.5$, $b/h_1 = 1.0$ and $\rho_3/\rho_1 = 1.0$. As expected, the peaks are greater for smaller μ_3/μ_1, but suppressed below that of the homogeneous strip when $\mu_3/\mu_1 > 1.0$, owing to the constraint from the adjacent

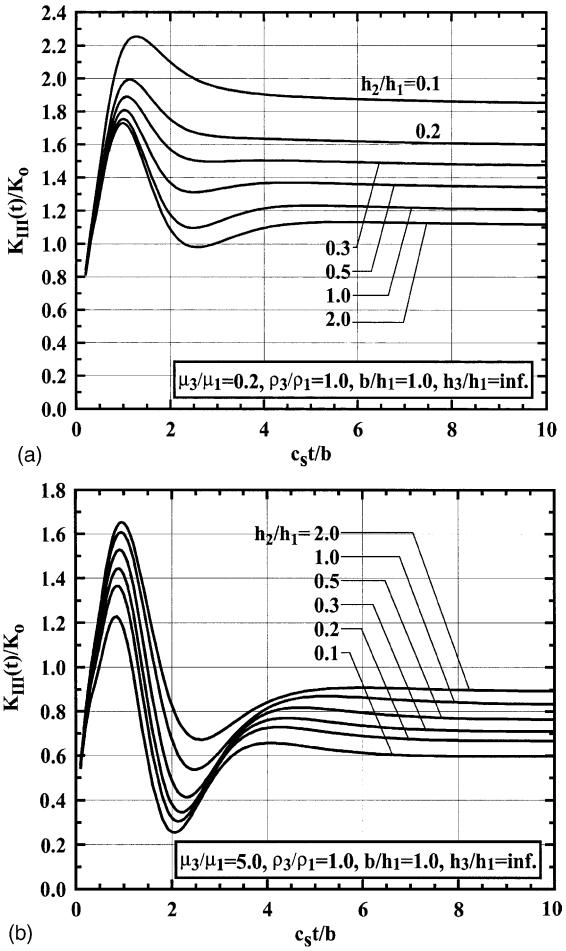

Fig. 4. Normalized dynamic stress intensity factors $K_{III}(t)/K_0$ of an edge crack as a function of dimensionless time $c_s t/b$ for different values of h_2/h_1 ($K_0 = \tau_0 b^{1/2}$, (a) $\mu_3/\mu_1 = 0.2$, (b) $\mu_3/\mu_1 = 5.0$, $\rho_3/\rho_1 = 1.0$, $b/h_1 = 1.0$, $h_3/h_1 = \infty$).

stiffer substrate. Another point to be noted is that the peak magnitude in the dynamic stress intensification and the elapsed time interval before it occurs appear to be hardly affected by the substrate thickness h_3/h_1, although the static solutions may be lowered as h_3/h_1 is increased. Table 2 shows that the effect of inertia as measured by the ratio $(K_{III})_{peak}/(K_{III})_{static}$ is more notable for the substrate of greater stiffness and thickness, and that the shear modulus ratio is more influential than the substrate thickness.

Figures 4a and b contain the plots of time variations of the dynamic stress intensity factors for different values of interlayer thickness h_2/h_1, where it is prescribed that $\rho_3/\rho_1 = 1.0$, $b/h_1 = 1.0$, and the substrate is semi-infinite as $h_3/h_1 = \infty$. Specifically, as shown in Fig. 4a, when $\mu_3/\mu_1 = 0.2$, the peak stress intensification tends to be lowered as h_2/h_1 is increased. Such a trend with respect to h_2/h_1 is indicative of the fact that the graded interlayer of greater thickness is more effective in alleviating the severity of edge cracking in the stiffer coating layer. In Fig. 4b, the opposite response is observed for $\mu_3/\mu_1 = 5.0$, where the amplitude of the curve drops as the interlayer is rendered thinner. It is noted that the solutions for the given material combinations are close to that for a homogeneous half-plane when $h_2/h_1 > 2.0$ so that the influence of the interlayer becomes insignificant. The dynamic overshoot of the stress intensity factors in Table 3 depicts

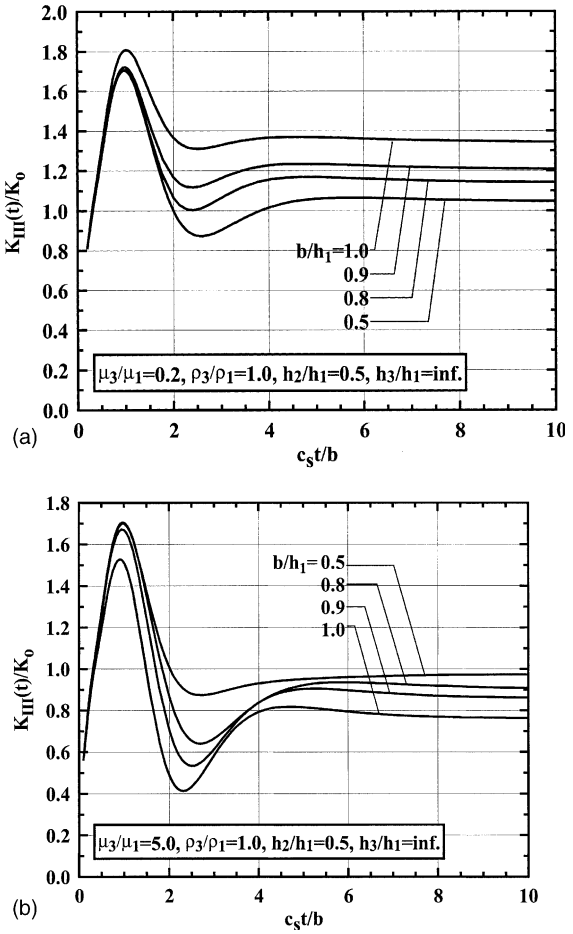

Fig. 5. Normalized dynamic stress intensity factors $K_{III}(t)/K_0$ of an edge crack as a function of dimensionless time $c_s t/b$ for different values of b/h_1 ($K_0 = \tau_0 b^{1/2}$, (a) $\mu_3/\mu_1 = 0.2$, (b) $\mu_3/\mu_1 = 5.0$, $\rho_3/\rho_1 = 1.0$, $h_2/h_1 = 0.5$, $h_3/h_1 = \infty$).

that for the coating stiffer than the substrate as $\mu_3/\mu_1 = 0.2$, the more remarkable effect of inertia exists for the greater h_2/h_1, whereas the opposite is true when $\mu_3/\mu_1 = 5.0$.

With $\rho_3/\rho_1 = 1.0$, $h_2/h_1 = 0.5$, and $h_3/h_1 = \infty$, Figure 5a demonstrates that for the stiff coating as $\mu_3/\mu_1 = 0.2$ the peak value of the stress intensity factors becomes greater when the crack size b/h_1 is increased, while Figure 5b shows the reverse tendency for the case of compliant coating as $\mu_3/\mu_1 = 5.0$. Besides, it can be conjectured that for $b/h_1 < 0.5$, the dynamic stress intensity factors are closely matched with those of an edge-cracked homogeneous medium. In Table 4, the dynamic overshoot characteristics are also described in terms of $(K_{III})_{peak}/(K_{III})_{static}$, from which it is inferable that the inertia effect is more appreciable for the smaller crack size when $\mu_3/\mu_1 = 0.2$ and the opposite prevails when $\mu_3/\mu_1 = 5.0$.

How the mass density ratio ρ_3/ρ_1 affects the dynamic crack-tip response is next examined for two different values of shear modulus ratio μ_3/μ_1, where it is assumed that $h_2/h_1 = 0.5$, $b/h_1 = 1.0$, and $h_3/h_1 = \infty$. Figure 6a predicts that when $\mu_3/\mu_1 = 0.2$, the severity of near-tip region tends to be somewhat attenuated as ρ_3/ρ_1 is increased. When $\mu_3/\mu_1 = 5.0$, the reverse behavior is plotted in Fig. 6b such that the constraint by the nearby stiffer substrate can be offset by increasing ρ_3/ρ_1. Moreover, the effect of ρ_3/ρ_1 on the dynamic stress intensity factors is observed to be more discernible when the coating layer is stiffer than

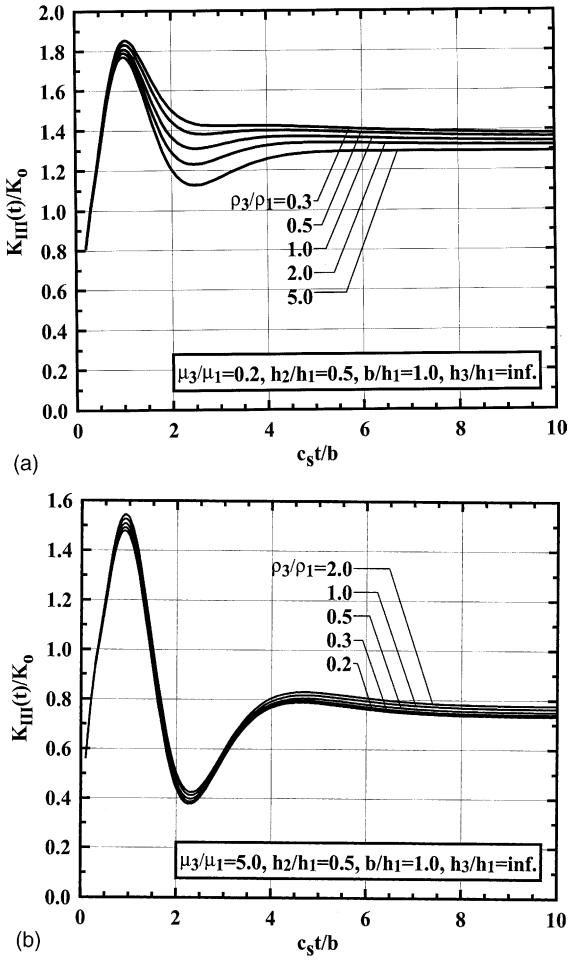

Fig. 6. Normalized dynamic stress intensity factors $K_{III}(t)/K_0$ of an edge crack as a function of dimensionless time $c_s t/b$ for different values of ρ_3/ρ_1 ($K_0 = \tau_0 b^{1/2}$, (a) $\mu_3/\mu_1 = 0.2$, (b) $\mu_3/\mu_1 = 5.0$, $h_2/h_1 = 0.5$, $b/h_1 = 1.0$, $h_3/h_1 = \infty$).

Table 1
Ratios between the peak and elastostatic stress intensity factors, $(K_{III})_{peak}/(K_{III})_{static}$, for a homogeneous strip containing a center or an edge crack

	$2c/h$							
	0.1	0.2	0.3	0.4	0.5	0.6	0.7	0.8
Center crack	1.216	1.201	1.176	1.135	1.080	1.032	1.000	1.000
Edge crack	1.697	1.676	1.639	1.585	1.513	1.413	1.277	1.121

the substrate as in Fig. 6a. The overall effect of ρ_3/ρ_1, however, appears to be less appreciable when compared with that of μ_3/μ_1 in Fig. 3. Because the static solutions are independent of the mass density, Table 5 delineates that for $\mu_3/\mu_1 = 0.2$, the inertia effect becomes more noticeable when ρ_3/ρ_1 is lowered.

Table 2
Ratios between the peak and elastostatic stress intensity factors, $(K_{III})_{peak}/(K_{III})_{static}$, of an edge crack for different values of μ_3/μ_1 and h_3/h_1 ($h_2/h_1 = 0.5$, $b/h_1 = 1.0$, $\rho_3/\rho_1 = 1.0$)

	μ_3/μ_1				
	0.2	0.5	1.0	2.0	5.0
$h_3/h_1 = 1.0$	1.246	1.419	1.585	1.755	1.943
$h_3/h_1 = 1.5$	1.270	1.455	1.623	1.788	1.963
$h_3/h_1 = \infty$	1.364	1.552	1.704	1.846	1.994

Table 3
Ratios between the peak and elastostatic stress intensity factors, $(K_{III})_{peak}/(K_{III})_{static}$, of an edge crack for different values of h_2/h_1 and μ_3/μ_1($\rho_3/\rho_1 = 1.0$, $b/h_1 = 1.0$, $h_3/h_1 = \infty$)

	h_2/h_1					
	0.1	0.2	0.3	0.5	1.0	2.0
$\mu_3/\mu_1 = 0.2$	1.238	1.265	1.299	1.364	1.469	1.561
$\mu_3/\mu_1 = 5.0$	2.048	2.039	2.025	1.994	1.930	1.860

Table 4
Ratios between the peak and corresponding elastostatic stress intensity factors, $(K_{III})_{peak}/(K_{III})_{static}$, of an edge crack for different values of b/h_1 and μ_3/μ_1 ($\rho_3/\rho_1 = 1.0$, $h_2/h_1 = 0.5$, $h_3/h_1 = \infty$)

	b/h_1			
	0.5	0.8	0.9	1.0
$\mu_3/\mu_1 = 0.2$	1.640	1.509	1.441	1.364
$\mu_3/\mu_1 = 5.0$	1.756	1.877	1.941	1.994

Table 5
Ratios between the peak and elastostatic stress intensity factors, $(K_{III})_{peak}/(K_{III})_{static}$, of an edge crack for different values of ρ_3/ρ_1 and μ_3/μ_1 ($h_2/h_1 = 0.5$, $b/h_1 = 1.0$, $h_3/h_1 = \infty$)

	ρ_3/ρ_1			
	0.3	0.5	1.0	2.0
$\mu_3/\mu_1 = 0.2$	1.398	1.382	1.364	1.350
$\mu_3/\mu_1 = 5.0$	1.949	1.969	1.994	2.016

6. Closure

The elastodynamic response of a surface crack in a coating/substrate system with a functionally graded interfacial zone has been investigated under the condition of antiplane shear impact. The interfacial zone was modeled by a nonhomogeneous interlayer that possesses the power-law variations of shear modulus and mass density. The integral transform techniques were employed and a singular integral equation with a generalized Cauchy kernel was derived in the Laplace transform domain. As the main results, the evolution of the dynamic mode III stress intensity factors with time and the overshoot characteristics were presented for various material and geometric combinations of the coating/substrate system with the interlayer. Specifically, it was illustrated that the values of the dynamic stress intensity factors are markedly influenced by the shear modulus ratio, the interlayer thickness, and the crack size as well, but are dependent to a lesser

degree on the substrate thickness and the mass density ratio. Of particular interest was that the peak magnitude of the dynamic stress intensity factors appears to be unaffected by the substrate thickness. Furthermore, the inertia effect, as measured by the ratio between the peak value of the dynamic stress intensity factors and the corresponding elastostatic solution, may become more pronounced for the compliant coating or for the substrate of greater stiffness and thickness. On the other hand, such an inertia effect was shown to either increase or decrease as the interlayer thickness, the crack size, and the mass density ratio are increased, depending on the stiffness of the substrate relative to that of the coating.

Acknowledgements

This work was supported by the Basic Research Program of the Korea Science and Engineering Foundation, Republic of Korea, under the grant no. R01-2003-000-10341-0. The support is gratefully acknowledged.

Appendix A

The function $\Delta_0(s,p)$ in Eq. (28) is written as

$$\Delta_0(s,p) = \frac{f_{22}g_1 - f_{21}g_2}{f_{11}f_{22} - f_{12}f_{21}}, \tag{A.1}$$

where $f_{ij}(s,p)$, $i,j = 1,2$, and $g_i(s,p)$, $i = 1,2$, are expressed as

$$f_{11}(s,p) = \delta_1 I_v\left(\frac{s}{|\alpha|}\right) + 2\delta_2\left[I_{v+1}\left(\frac{s}{|\alpha|}\right) + \frac{v|\alpha|}{s} I_v\left(\frac{s}{|\alpha|}\right)\right], \tag{A.2}$$

$$f_{12}(s,p) = \delta_1 K_v\left(\frac{s}{|\alpha|}\right) - 2\delta_2\left[K_{v+1}\left(\frac{s}{|\alpha|}\right) - \frac{v|\alpha|}{s} K_v\left(\frac{s}{|\alpha|}\right)\right], \tag{A.3}$$

$$f_{21}(s,p) = \delta_3 I_v\left[\frac{s}{|\alpha|}(1+\alpha h_2)\right] + 2\delta_4\left[I_{v+1}\left[\frac{s}{|\alpha|}(1+\alpha h_2)\right] + \frac{v|\alpha|}{s(1+\alpha h_2)} I_v\left[\frac{s}{|\alpha|}(1+\alpha h_2)\right]\right], \tag{A.4}$$

$$f_{22}(s,p) = \delta_3 K_v\left[\frac{s}{|\alpha|}(1+\alpha h_2)\right] - 2\delta_4\left[K_{v+1}\left[\frac{s}{|\alpha|}(1+\alpha h_2)\right] - \frac{v|\alpha|}{s(1+\alpha h_2)} K_v\left[\frac{s}{|\alpha|}(1+\alpha h_2)\right]\right], \tag{A.5}$$

$$g_1(s,p) = \left[1 + \left(\frac{1-\beta}{2}\right)\frac{\alpha}{\lambda_1}\right] I_v\left(\frac{s}{|\alpha|}\right) + \frac{\alpha}{|\alpha|}\frac{s}{\lambda_1}\left[I_{v+1}\left(\frac{s}{|\alpha|}\right) + \frac{v|\alpha|}{s} I_v\left(\frac{s}{|\alpha|}\right)\right], \tag{A.6}$$

$$g_2(s,p) = \left[1 + \left(\frac{1-\beta}{2}\right)\frac{\alpha}{\lambda_1}\right] K_v\left(\frac{s}{|\alpha|}\right) - \frac{\alpha}{|\alpha|}\frac{s}{\lambda_1}\left[K_{v+1}\left(\frac{s}{|\alpha|}\right) - \frac{v|\alpha|}{s} K_v\left(\frac{s}{|\alpha|}\right)\right], \tag{A.7}$$

together with $\delta_j(s,p)$, $j = 1,\ldots,4$, given by

$$\delta_1(s,p) = -2\sinh\lambda_1 h_1 + \frac{(1-\beta)\alpha}{\lambda_1}\cosh\lambda_1 h_1, \tag{A.8}$$

$$\delta_2(s,p) = \frac{\alpha}{|\alpha|}\frac{s}{\lambda_1}\cosh\lambda_1 h_1, \tag{A.9}$$

$$\delta_3(s,p) = 2(1+\alpha h_2)^{(1-\beta)/2}\sinh\lambda_3 h_3 + \frac{(1-\beta)\alpha}{\lambda_3}(1+\alpha h_2)^{(1+\beta)/2}\cosh\lambda_3 h_3, \tag{A.10}$$

$$\delta_4(s,p) = \frac{\alpha}{|\alpha|}\frac{s}{\lambda_3}(1+\alpha h_2)^{(1-\beta)/2}\cosh\lambda_3 h_3. \tag{A.11}$$

It is noted that when the substrate is treated as a semi-infinite constituent such that $h_3 \to \infty$, the regularity condition $w_3(+\infty, y, t) = 0$ is to be enforced, instead of the traction-free condition in the second of Eq. (7). In this case, it can be shown that the expressions in Eqs. (A.1)–(A.9) remain unaltered, but those in Eqs. (A.10) and (A.11) are replaced by the followings:

$$\delta_3(s,p) = (1+\alpha h_2)^{(1-\beta)/2} + \frac{(1-\beta)\alpha}{2\lambda_3}(1+\alpha h_2)^{(1+\beta)/2}, \tag{A.12}$$

$$\delta_4(s,p) = \frac{\alpha}{2|\alpha|}\frac{s}{\lambda_3}(1+\alpha h_2)^{(1-\beta)/2}. \tag{A.13}$$

References

Babaei, R., Lukasiewicz, S.A., 1998. Dynamic response of a crack in a functionally graded material between two dissimilar half-planes under anti-plane shear impact load. Engineering Fracture Mechanics 60, 479–487.

Chen, E.P., 1977. Impact response of a finite crack in a finite strip under anti-plane shear. Engineering Fracture Mechanics 9, 719–724.

Chen, J., Liu, Z., Zou, Z.Z., 2002. Transient internal crack problem for a nonhomogeneous orthotropic strip (Mode I). International Journal of Engineering Science 40, 1761–1774.

Chiu, T.-C., Erdogan, F., 1999. One-dimensional wave propagation in a functionally graded elastic medium. Journal of Sound and Vibration 222, 453–487.

Churchill, R.V., 1981. Operational Mathematics, third ed. McGraw-Hill, New York.

Davis, P.J., Rabinowitz, P., 1984. Methods of Numerical Integration, second ed. Academic Press, New York.

Eischen, J.W., 1987. Fracture of nonhomogeneous materials. International Journal of Fracture 34, 3–22.

Erdogan, F., 1998. Crack Problems in Nonhomogeneous Materials. In: Cherepanov, G.P. (Ed.), Fracture, A Topical Encyclopedia of Current Knowledge. Krieger Publishing Company, Florida, pp. 72–98.

Feng, W.J., Zhang, Z.G., Zou, Z.Z., 2003. Impact failure prediction of Mode III crack in orthotropic functionally graded strip. Theoretical and Applied Fracture Mechanics 40, 97–104.

Gradshteyn, I.S., Ryzhik, I.M., 1980. Table of Integrals, Series, and Products. Academic Press, New York.

Itou, S., 2001. Transient dynamic stress intensity factors around a crack in a nonhomogeneous interfacial layer between two dissimilar elastic half-planes. International Journal of Solids and Structures 38, 3631–3645.

Jin, Z.-H., Noda, N., 1994. Crack-tip singular fields in nonhomogeneous materials. ASME Journal of Applied Mechanics 61, 738–740.

Li, C., Weng, G.J., 2002. Dynamic fracture analysis for a penny-shaped crack in an FGM interlayer between dissimilar half-spaces. Mathematics and Mechanics of Solids 7, 149–163.

Li, C., Weng, G.J., Duan, Z., 2001. Dynamic behavior of a cylindrical crack in a functionally graded interlayer under torsional loading. International Journal of Solids and Structures 38, 7473–7485.

Miyamoto, Y., Kaysser, W.A., Rabin, B.H., Kawasaki, A., Ford, R.G. (Eds.), 1999. Functionally Graded Materials: Design, Processing, and Applications. Kluwer Academic Publishers, Hingham, MA.

Murakami, Y. (Ed.), 1987. Stress Intensity Factors Handbook. Pergamon Press, New York.

Muskhelishvili, N.I., 1953. Singular Integral Equations. Noordhoff, Groningen, The Netherlands.

Sih, G.C., Chen, E.P., 1981. Mechanics of Fracture 6: Cracks in Composite Materials. Martinus Nijhoff Publishers, The Hague.

Stehfest, H., 1970. Numerical inversion of Laplace transforms. Communications of the ACM 13, 47–49, 624.

Suresh, S., Mortensen, A., 1998. Fundamentals of Functionally Graded Materials. The Institute of Materials, London.

Wang, B.L., Han, J.C., Du, S.Y., 2000. Cracks problem for non-homogeneous composite material subjected to dynamic loading. International Journal of Solids and Structures 37, 1251–1274.

Wang, Y.S., Gross, D., 2000. Analysis of a crack in a functionally gradient interface layer under static and dynamic loading. Key Engineering Materials 183–187, 331–336.

Zhang, Ch., Sladek, J., Sladek, V., 2003. Effects of material gradients on transient dynamic mode-III stress intensity factors in an FGM. International Journal of Solids and Structures 40, 5251–5270.